Microsyst Technol (2012) 18:1651–1660
DOI 10.1007/s00542-012-1603-0

TECHNICAL PAPER

Design and experimental validation of a sliding-mode stabilizer for a ship-carried satellite antenna

Paul C.-P. Chao · Chun-Wei Chiu

Received: 30 September 2011 / Accepted: 14 June 2012 / Published online: 15 July 2012

Abstract This study designs a sliding-mode controller to stabilize the angular orientation of a ship-carried satellite antenna. The design process starts with calculating the pointing angle of the considered satellite antenna arm as opposed to given ship vibrations due to certain sea waves. This calculation is carried out by the method of Denavit–Hartenberg (D–H) transformation, which is followed by establishing a dynamic model of the satellite antenna system and platform using conventional kinematics modeling techniques. The resulted kinematics relationships are next used as the basis for designing a sliding-mode controller to maintain the antenna in a specified orientation as the ship pitches and rolls under the combined effects of wind and the sea's waves. The effectiveness of the designed controller is investigated both numerically and experimentally. Both sets of results confirm the feasibility of the proposed control scheme. It is shown that the antenna converges to the required azimuth and elevation angles within 2 s and maintains the specified orientation as the ship continues to pitch and roll.

List of symbols

A	Amplitude of oscillation
a	Cylinder diameter
B	Vector of the Coriolis and centrifugal forces
C_p	Pressure coefficient
Cx	Force coefficient in x direction
Cy	Force coefficient in y direction
c	Chord
d	Vector of the disturbance
dt	Time step
e	Tracking error
Fx	X component of resultant pressure force acting on vehicle
Fy	Y component of resultant pressure force acting on vehicle
f, g	Generic functions
G	Vector of the gravitational force
h	Height
i	Time index during navigation
j	Waypoint index
K	Trailing-edge (TE) non-dimensional angular deflection rate
L	Lagrange function
M	Inertia matrix
q	A vector containing the joint angles
S	Sliding surface function
T	Denavit–Hartenberg (D–H) transformation
u	The unit directional vector
V	Lyapunov function
θ_2, θ_3	Roll and pitch angles of the hydraulic platform, respectively
θ_4, θ_5	Angles of arm-1 and arm-2, respectively
$\boldsymbol{\tau}$	Vector of the torque input

P. C.-P. Chao (✉)
Department of Electrical Engineering, National Chiao Tung University, Hsinchu 300, Taiwan
e-mail: pchao@mail.nctu.edu.tw

C.-W. Chiu
Department of Mechanical Engineering, Chung Yuan Christian University, Chungli, Taiwan

1 Introduction

While a ship traveling across the sea, wind and the sea's waves cause it to experience irregular 3-D motions. A satellite dish used mounted on the ship's structure and used for navigation purposes must maintain steady orientations

along directions of azimuth and elevation in order to ensure the quality of the signals received from a global positioning satellite. Tracking control of the ship-mounted antenna is much challenging as the ship is constantly in 3-D motions (including rolling and pitching), since the sensed signals would involve noise. To achieve tracking control of the satellite dish in required quality level. Dynamic modeling and subsequent control design are carried out by this study. The dynamic motion of a ship is essentially nonlinear and with six degrees of freedom (DOF) (Chen 1993; Chris Tseng and Teo Dennis 1998). In stabilizing the orientation of the antenna dish, the ship motions of particular concern are the yaw, pitch and roll displacements. To compensate for these motions such that the antenna dish remains aligned toward to the positioning satellite in the sky at all times, the antenna must be capable of moving independently of the ship's structure. Accordingly, the present study constructs a two-armed robotic system to support the antenna dish and to adjust its physical orientation (Spong and Vidyasagar 1989). The orientation of the dish is maintained in the desired position by using a sliding-mode controller to regulate the trajectories of the two arms as the ship pitches and rolls.

The design of sliding-mode controllers is well documented in the literature. For example, Young (1978) and Slotine (1984) applied sliding-mode controllers to regulate the response of simple, non-linear robotic systems. However, in both studies, the controller design was complex and required the inverse of the inertia matrix to be calculated. Accordingly, Yeung and Chen (1988) and Chen et al. (1990) proposed simplified algorithms for sliding-mode controllers. The current study applies the same simplified approach to construct a sliding-mode controller to regulate the trajectories of the robotic arms supporting the satellite antenna dish. Figure 1 presents a conceptual illustration of controlling a ship-carried satellite antenna in this study to demonstrate the feasibility of the proposed sliding-mode controller. Figure 2 shows the photo of the corresponding physical system, while Fig. 3 gives a schematic with varied parameters defined. As shown in Figs. 2 and 3, the antenna dish is attached to a two-DOF robot mounted on a triangular platform supported by a rod with a universal joint at one corner and two hydraulic cylinders at the other two corners. The platform itself plays the role of the ship body. Roll and pitch motions of the ship are simulated by supplying appropriate driving signals to the AC motors used to actuate two cylinders, for the purpose of realizing corresponding roll and pitch angles of the platform that supporting the antenna dish. The displacements of the two hydraulic cylinders are measured using linear potentiometers.

It is seen from the illustration given in Fig. 1 that sea waves cause certain types of pitch and roll motions of the ship. These pitch and roll motions are simulated in the

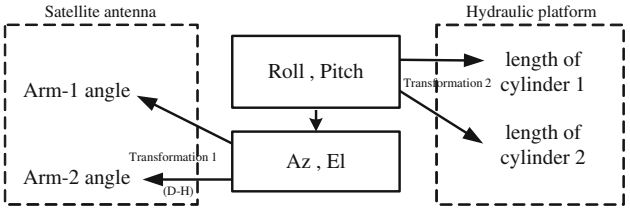

Fig. 1 Conceptual illustration of controlling the satellite antenna

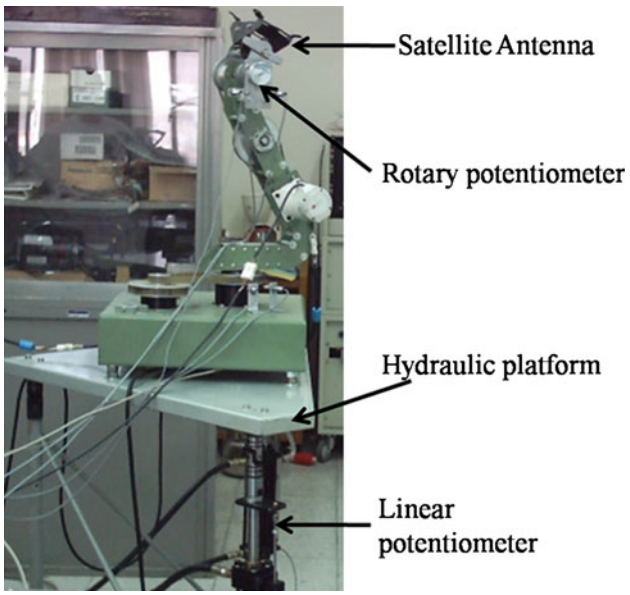

Fig. 2 Photograph of the satellite antenna mounted on hydraulic platform

laboratory by the displacements of the two cylinders in the satellite platform constructed by this study. The required cylinder displacements are calculated based on the established Transformation 2, as illustrated by this figure, based on pitch and roll motions of the ship. On the other hand, the information of the ship pitch and roll are provided to find the global pointing angle of the antenna relative to ground—Az and El, which are then used to compute the desired arm angles (Arm 1 and 2) for the antenna robot via Transformation 1.

The remainder of this study is organized as follows. Section 2 analyzes the kinematics of the antenna/hydraulic platform system. Subsection 2 A realizes Transformation 2 in Fig. 2 via the known Denavit–Hartenberg (D–H) transformation, while subsection 2 B does Transformation 1 in Fig. 1. Section 3 uses the resulting kinematics expressions to construct the governing equations of the antenna dish. Based upon this dynamic model, Sect. 4 develops a robust sliding-mode controller to regulate the position of the antenna dish as the hydraulic platform performs roll and pitch motions. Section 5 presents the results of a series of numerical and experimental trials designed to verify the

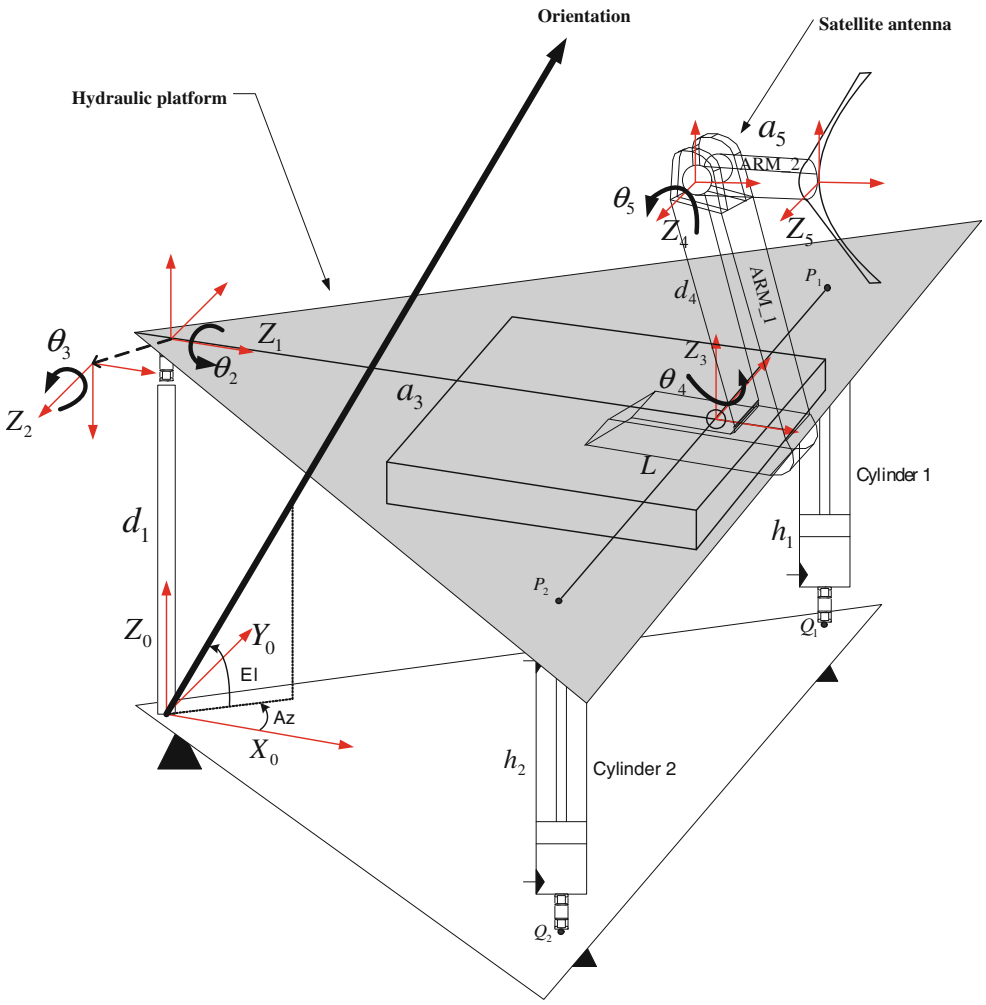

Fig. 3 Relationship between the satellite antenna and hydraulic platform

performance of the proposed control scheme. Finally, Sect. 6 provides some brief concluding remarks and indicates the intended direction of future research.

2 Kinematics analysis

2.1 From platform to angular orientation of the antenna

Table 1 summarizes the major kinematics parameters of the satellite antenna/hydraulic platform system shown in Fig. 1. This section establishes the relationship between the angles of the two arms of the robot supporting the antenna dish and the azimuth and elevation angles of the dish relative to the Earth as the hydraulic platform performs pitch and roll motions. The kinematics relationships of the antenna/platform system enable appropriate angles of the two robotic arms to be computed to maintain the antenna dish in the specified orientation as the roll and pitch angles of the platform vary dynamically.

Table 1 Kinematics parameters for satellite antenna and hydraulic platform

	θ	d	a	α	Home
1	0	d_1	0	$\pi/2$	$\pi/2$
2	θ_2	0	0	$\pi/2$	$-\pi/2$
3	θ_3	0	a_3	$-\pi/2$	$\pi/2$
4	θ_4	d_4	0	$\pi/2$	0
5	θ_5	0	a_5	0	0

In this study, the relationship between the angles of the two robotic arms and the azimuth and elevation angles of the antenna dish as the platform pitches and rolls are established using the conventional Denavit–Hartenberg (D–H) transformation method (Robert 1990). According to this method, the transformation from coordinate frame 0 (i.e. the ground coordinate framework) to coordinate frame 3 (i.e. the frame fixed to the foundation of the satellite antenna) has the form

$$\mathbf{T}_{\mathbf{0}}^{\mathbf{3}} = \begin{bmatrix} \cos\theta_3 & 0 & -\sin\theta_3 & a_3\cos\theta_3 \\ -\sin\theta_2\sin\theta_3 & \cos\theta_2 & -\sin\theta_2\cos\theta_3 & -a_3\sin\theta_2\sin\theta_3 \\ \cos\theta_2\sin\theta_3 & \sin\theta_2 & \cos\theta_2\cos\theta_3 & a_3\cos\theta_2\sin\theta_3 + d_1 \\ 0 & 0 & 0 & 1 \end{bmatrix}, \tag{1}$$

where θ_2 and θ_3 are the roll and pitch angles of the hydraulic platform, respectively. Meanwhile, the transformation from coordinate frame 3 to coordinate frame 5 (i.e. the frame fixed to the end point of the robot's upper arm (i.e. arm-2) attached to the center of the antenna dish) is given by

$$\mathbf{T}_{\mathbf{3}}^{\mathbf{5}} = \begin{bmatrix} \cos\theta_4\cos\theta_5 & -\cos\theta_4\sin\theta_5 & \sin\theta_4 & a_5\cos\theta_4\cos\theta_5 \\ \sin\theta_4\cos\theta_5 & -\sin\theta_4\sin\theta_5 & -\cos\theta_4 & a_5\sin\theta_4\cos\theta_5 \\ \sin\theta_5 & \cos\theta_5 & 0 & a_5\sin\theta_5 + d_4 \\ 0 & 0 & 0 & 1 \end{bmatrix}, \tag{2}$$

where θ_4 and θ_5 are the angles of arm-1 and arm-2, respectively. The relationship between the end point of arm-2 and the Earth can then be defined as

$$\mathbf{T}_{\mathbf{0}}^{\mathbf{5}} = \mathbf{T}_{\mathbf{0}}^{\mathbf{3}}\mathbf{T}_{\mathbf{3}}^{\mathbf{5}}. \tag{3}$$

As shown in Fig. 2, the antenna dish points along the X_5 axis direction. Let $\mathbf{u}_5 = [1 \quad 0 \quad 0 \quad 1]^T$ be the unit directional vector at associated with coordinate frame 5. Furthermore, let $\mathbf{A}(\theta_2, \theta_3) = \mathbf{T}_0^3$ and $\mathbf{F}(\theta_4, \theta_5) = \mathbf{T}_3^5$, respectively. The pointing direction of the antenna dish relative to coordinate frame 0 can therefore be described by the following unit vector

$$\mathbf{u}_0 = \mathbf{T}_0^5 \cdot \mathbf{u}_5 = \mathbf{A}(\theta_2, \theta_3) \cdot \mathbf{F}(\theta_4, \theta_5) \cdot \mathbf{u}_5. \tag{4}$$

Given the required azimuth angle (Az) and elevation angle (El) of the antenna dish relative to the Earth's coordinate framework (i.e. $X_0Y_0Z_0$), the corresponding direction of the dish can be expressed in terms of the following unit vector (Chris Tseng and Teo Dennis 1998)

$$\mathbf{u}_0(Az, El) = \begin{bmatrix} \cos Az\cos El \\ \sin Az\cos El \\ \sin El \\ 1 \end{bmatrix}. \tag{5}$$

Substituting Eq. (5) into Eq. (4) yields

$$\mathbf{F}(\theta_4, \theta_5) \cdot \mathbf{u}_5 = \mathbf{A}^{-1} \cdot \mathbf{u}_0. \tag{6}$$

The next step is to solve the above equation for θ_4 and θ_5, two arm angles relative to platform, with a known $\mathbf{u}_0$ from given azimuth (Az) and elevation angles (El) of the antenna relative to ground, and also a known $\mathbf{u}_5$ from assumed ship vibration caused by sea waves. The solved θ_4 and θ_5 will be used in the next section to find required displacements of supporting hydraulic cylinders to attain theses particular values of θ_4 and θ_5.

2.2 From hydraulic cylinders to platform

As shown in Fig. 1, the platform used to simulate the ship's structure has a triangular form with one corner pinned and the other two corners, i.e. points P_1 and P_2, supported/driven by two hydraulic cylinders. During the experiments, the displacements of the two cylinders are regulated by a programmable controller in such a way that the platform reproduces typical roll and pitch motions of a ship at sea.

This section derives the kinematics relationships between the cylinder displacements and the roll/pitch angles of the platform. The resulting expressions enable appropriate cylinder displacements to be computed to reproduce specific roll and pitch motions.

The coordinates of points P_1 and P_2 relative to coordinate framework 3 are given as follows

$${}^3P_1 = \begin{bmatrix} 0 & L/2 & 0 & 1 \end{bmatrix}^T,$$

$${}^3P_2 = \begin{bmatrix} 0 & -L/2 & 0 & 1 \end{bmatrix}^T.$$

where "3" denotes the frame in which P_1 and P_2 are described, and L is the distance between the two points. Meanwhile, the coordinates of points P_1 and P_2 relative to coordinate framework 0 are given by

$$\begin{bmatrix} {}^0P_i \end{bmatrix} = \mathbf{T}_0^3 \begin{bmatrix} {}^3P_i \end{bmatrix}, \quad i = 1, 2. \tag{7}$$

where $\mathbf{T}_{\mathbf{0}}^{\mathbf{3}}$ is defined in Eq. (1). From Eq. (7), it can be shown that

$$\begin{bmatrix} {}^0P_{1x} \\ {}^0P_{1y} \\ {}^0P_{1z} \\ 1 \end{bmatrix} = \begin{bmatrix} a_3\cos\theta_3 \\ \frac{1}{2}L\cos\theta_2 - a_3\sin\theta_2\sin\theta_3 \\ \frac{1}{2}L\sin\theta_2 + a_3\cos\theta_2\sin\theta_3 + d_1 \\ 1 \end{bmatrix}, \tag{8}$$

$$\begin{bmatrix} {}^0P_{2x} \\ {}^0P_{2y} \\ {}^0P_{2z} \\ 1 \end{bmatrix} = \begin{bmatrix} a_3\cos\theta_3 \\ -\frac{1}{2}L\cos\theta_2 - a_3\sin\theta_2\sin\theta_3 \\ -\frac{1}{2}L\sin\theta_2 + a_3\cos\theta_2\sin\theta_3 + d_1 \\ 1 \end{bmatrix}. \tag{9}$$

The positions of the connection points of the two hydraulic cylinders (i.e. points Q_1 and Q_2, respectively, see Fig. 1) relative to the ground framework are given by

$${}^0Q_1 = \begin{bmatrix} a_3 & L/2 & 0 & 1 \end{bmatrix}^T,$$

$${}^0Q_2 = \begin{bmatrix} a_3 & -L/2 & 0 & 1 \end{bmatrix}^T.$$

Clearly, the overall lengths of the two hydraulic cylinders are equivalent to the distances between points P_1 and Q_1 and P_2 and Q_2, respectively, i.e.

$$h_i(\theta_2, \theta_3) = \left\| {}^0P_i - {}^0Q_i \right\|, \quad i = 1, 2, \tag{10}$$

where h_1 and h_2 are functions of θ_2 and θ_3 since points P_1 and P_2 vary depending on the roll (θ_2) and pitch (θ_3) angles of the platform. Hence, given specified values of the pitch

and roll, Eq. (10) enables the appropriate displacements of the two hydraulic cylinders to be obtained.

3 Dynamic model of satellite antenna

Based upon the kinematics relationships established in Sect. 2, this section of the paper uses the D–H transformation method and Lagrange equation to derive the governing equations of motion of the satellite antenna mounted on the hydraulic platform. According to basic dynamic principles, the total kinetic energy of the satellite antenna in Fig. 1 is equal to the sum of the individual kinetic energies of the two robotic arms (Robert 1990; Mark and Vidyasagar 1988), i.e.

$$\mathbf{T}(\mathbf{q},\dot{\mathbf{q}}) = \sum_{k=1}^{2} \frac{({}^k\bar{v})^T \mathbf{m}_k {}^k\bar{v} + ({}^k\bar{\omega})^T \mathbf{D}_k {}^k\bar{\omega}}{2}. \tag{11}$$

where $\mathbf{q}$ is a vector containing the joint angles (equivalent to angles θ_4 and θ_5), i.e. $\mathbf{q} = [\,\theta_4 \quad \theta_5\,]^T$; ${}^k\bar{v} \in \mathbf{R}^3$ denotes the velocity of the center of mass (CM) of arm k with respect to the ground; ${}^k\bar{\omega} \in \mathbf{R}^3$ denotes the angular velocity of the CM of arm k relative to the ground; m_k denotes the mass of arm k; and $\mathbf{D}_k$ is the 3×3 inertia tensor of arm k about its CM.

The total potential energy of the Lagrange is given by

$$\mathbf{U}(\mathbf{q}) = -\sum_{k=1}^{2} \mathbf{m}_k \mathbf{g}^T \bar{\mathbf{c}}^k(\mathbf{q}) \tag{12}$$

where $\bar{\mathbf{c}}^k$ denotes the CM of arm k with respect to the ground and $\mathbf{g}$ denotes the gravitational acceleration of arm k with respect to the ground.

The difference between the kinetic and potential energies of the antenna can be expressed using the following Lagrange function

$$\mathbf{L}(\mathbf{q},\dot{\mathbf{q}}) = \mathbf{T}(\mathbf{q},\dot{\mathbf{q}}) - \mathbf{U}(\mathbf{q}). \tag{13}$$

The equation of motion of the antenna can then be obtained by substituting the total energy in Eq. (13) into the Lagrange equation, i.e.

$$\frac{d}{dt}\frac{\partial}{\partial \dot{q}_i}\mathbf{L}(\mathbf{q},\dot{\mathbf{q}}) - \frac{\partial}{\partial q_i}\mathbf{L}(\mathbf{q},\dot{\mathbf{q}}) = \mathbf{F}_i, \quad i = 1,2, \tag{14}$$

where $\mathbf{F}_i$ is the generalized force acting on the ith joint. Hence, it can be shown that

$$\mathbf{M}(\mathbf{q})\ddot{\mathbf{q}} + \mathbf{B}(\mathbf{q},\dot{\mathbf{q}})\dot{\mathbf{q}} + \mathbf{G}(\mathbf{q}) = \boldsymbol{\tau}, \tag{15}$$

where $\mathbf{M}(\mathbf{q})$ is the inertia matrix, $\mathbf{B}(\mathbf{q},\dot{\mathbf{q}})\dot{\mathbf{q}}$ is the vector of the Coriolis and centrifugal forces, $\mathbf{G}(\mathbf{q})$ is the vector of the gravitational force, and $\boldsymbol{\tau}$ is the vector of the torque input. $\mathbf{M}(\mathbf{q})$, $\mathbf{B}(\mathbf{q},\dot{\mathbf{q}})\dot{\mathbf{q}}$ and $\mathbf{G}(\mathbf{q})$ are defined, respectively, as follows

$$\mathbf{M}(\mathbf{q}) = \begin{bmatrix} \frac{1}{3}m_5 a_5^2 \cos^2 q_2 + J_5 \sin^2 q_2 + J_4 & 0 \\ 0 & \frac{1}{3}m_5 a_5^2 \end{bmatrix}, \tag{16}$$

$$\mathbf{B} = \begin{bmatrix} -\sin 2q_2 (\frac{1}{3}m_5 a_5^2 - J_4)\dot{q}_1\dot{q}_2 \\ \frac{1}{2}\sin 2q_2 (\frac{1}{3}m_5 a_5^2 - J_4)\dot{q}_1^2 \end{bmatrix}, \tag{17}$$

$$\mathbf{G} = \begin{bmatrix} 0 \\ \frac{1}{2}a_5 m_5 g \cos q_2 \end{bmatrix}, \tag{18}$$

where m_5 and a_5 are the mass and length of arm-2 of the robotic structure, respectively, and J_4 and J_5 are the mass moments of inertia of arm-1 and arm-2, respectively.

4 Sliding-mode controller design

In order to obtain a robust control of the system, the dynamic equation of motion of the satellite antenna given in Eq. (15) can be expressed in the form

$$[\mathbf{M_0}(q) + \Delta\mathbf{M}(q)]\ddot{\mathbf{q}} + [\mathbf{B_0}(q,\dot{q}) + \Delta\mathbf{B}(q,\dot{q})]\dot{\mathbf{q}} + [\mathbf{G_0}(q) + \Delta\mathbf{G}] = \tau + \mathbf{d}, \tag{19}$$

where $\mathbf{d}$ is the vector of the disturbance, $\{\mathbf{M}_0, \mathbf{B}_0, \mathbf{G}_0\}$ are nominals of $\{\mathbf{M}, \mathbf{B}, \mathbf{G}\}$, and $\{\Delta\mathbf{M}, \Delta\mathbf{B}, \Delta\mathbf{G}\}$ are the assumed variations of $\mathbf{M}$, $\mathbf{B}$ and $\mathbf{G}$, with bounds satisfying

$$\begin{aligned} \|\Delta\mathbf{M}(q)\| &\le \boldsymbol{\delta}_{\mathbf{M}}, \\ \|\Delta\mathbf{B}(q,\dot{q})\| &\le \boldsymbol{\delta}_{\mathbf{B}}, \\ \|\Delta\mathbf{G}(q)\| &\le \boldsymbol{\delta}_{\mathbf{G}}, \\ \|\mathbf{d}\| &\le \boldsymbol{\delta}_{\mathbf{d}}. \end{aligned} \tag{20}$$

The system equation given in Eq. (20) is suitable for the design of a robust sliding-mode controller. Figure 4 presents a block diagram of the control scheme, in which the desired trajectory is defined by

$$\mathbf{q}_d = [\,q_{d1} \quad q_{d2}\,]^T, \tag{21}$$

and can be derived from Eq. (6). Furthermore, the tracking error is given by

$$\mathbf{e} = \mathbf{q} - \mathbf{q_d}. \tag{22}$$

Finally, the sliding surface has the form

$$\mathbf{S} = \mathbf{Ce} + \dot{\mathbf{e}}, \quad \mathbf{C} > 0, \tag{23}$$

where $\mathbf{C} = diag[\,c_1 \quad c_2\,]$, in which both c_1 and c_2 are positive.

The stability of the system is ensured via the following positive-definite Lyapunov function

$$V = \frac{1}{2}\mathbf{S^T M S}. \tag{24}$$

Differentiating V with respect to time and incorporating Eqs. (15), (22) and (23) gives

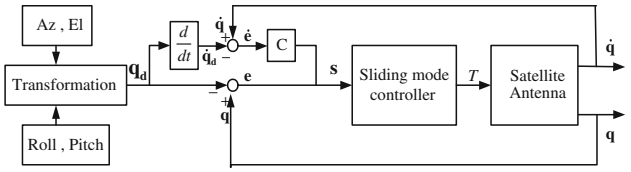

Fig. 4 Block diagram of the sliding-mode controller for satellite antenna

$$\dot{V} = \mathbf{S}^T[\mathbf{M}\mathbf{C}\dot{\mathbf{e}} + \boldsymbol{\tau} + \mathbf{d} - \mathbf{B} - \mathbf{G} - \mathbf{M}\ddot{\mathbf{q}}_d] + \frac{1}{2}\mathbf{S}^T(\dot{\mathbf{M}})S. \tag{25}$$

To ensure that the tracking error converges to the sliding surface, i.e. $\mathbf{S} = \mathbf{0}$, the control input, τ, must be designed such that V satisfies the condition

$$\dot{V} \leq 0. \tag{26}$$

Thus, τ is designed as

$$\boldsymbol{\tau} = -\mathbf{M}_0[\mathbf{C}\dot{\mathbf{e}} - \ddot{\mathbf{q}}_d] + \mathbf{B}_0 + \mathbf{G}_0 - \mathbf{P}\mathbf{S} - \mathbf{K}\mathrm{sgn}(\mathbf{S}), \tag{27}$$

where $\mathbf{P} = diag[p_1 \quad p_2]$ and $\mathbf{K} = diag[k_1 \quad k_2]$. The upper-bound of $\dot{M}/2$ is assumed to satisfy

$$\left\|\dot{\mathbf{M}}/2\right\| \leq \boldsymbol{\delta}_{\dot{\mathbf{M}}}/2, \tag{28}$$

and

$$p_i = \sum_{j=1}^{2} \delta_{\dot{M}_{ij}}/2, \tag{29}$$

$$k_i = \sum_{j=1}^{2} \delta_{M_{ij}}\left|c_j\dot{e}_j - \ddot{q}_{d_j}\right| + \delta_{B_i} + \delta_{G_i} + \delta_{d_i} + \eta_i, \quad \eta_i > 0. \tag{30}$$

Substituting Eq. (27) into Eq. (25), $\dot{V}$ becomes

$$\dot{V} = \mathbf{S}^{\mathbf{T}}\{\Delta\mathbf{M}[\mathbf{C}\dot{\mathbf{e}} - \ddot{\mathbf{q}}_d] - \Delta\mathbf{B} - \Delta\mathbf{G} - \mathbf{K}\mathrm{sgn}(\mathbf{S})\} + \mathbf{S}^{\mathbf{T}}\left(\dot{\mathbf{M}}/2 - \mathbf{P}\right)\mathbf{S}. \tag{31}$$

From Eq. (20) and Eqs. (28–30), it can be shown that Eq. (31) satisfies

$$\dot{V} \leq -\boldsymbol{\eta}|\mathbf{S}|. \tag{32}$$

Therefore, the controller satisfies the Lyapunov stability criterion, i.e. the trajectory reaches the sliding surface within a finite period of time. The components of the control law defined in Eq. (27) have the form

$$\tau_i = -\sum_{j=1}^{2} M_{0ij}\left[c_j\dot{e}_j - \ddot{q}_{d_j}\right] + B_{0i} + G_{0i} - s_i\sum_{j=1}^{2}\delta_{\dot{M}_{ij}}/2 - \mathrm{sgn}(s_i)\left[\sum_{j=1}^{2}\delta_{M_{ij}}\left|c_j\dot{e}_j - \ddot{q}_{d_j}\right| + \delta_{B_i} + \delta_{G_i} + \delta_{d_i} + \eta_i\right]. \tag{33}$$

where

$$\mathbf{M}_0 = \begin{bmatrix} \frac{1}{6}m_5a_5^2 + \frac{1}{2}J_4 & 0 \\ 0 & \frac{1}{3}m_5a_5^2 \end{bmatrix},$$

$$\mathbf{B}_0 = \begin{bmatrix} 0 \\ 0 \end{bmatrix},$$

$$\mathbf{G}_0 = \begin{bmatrix} 0 \\ \frac{1}{2}a_5gm_5\cos q_2 \end{bmatrix};$$

Someδ's can be determined from (Bailey and Arapostathis 1987)

$$|\Delta M_{11}| \leq \frac{1}{3}m_5a_5^2 + J_4 \triangleq \delta_{M_{11}},$$

$$|\Delta M_{12}| = |M_{21}| = 0,$$

$$|\Delta M_{22}| \leq \frac{1}{3}m_5a_5^2 \triangleq \delta_{M_{22}}.$$

Assuming that $\dot{q}$ is uniformly bounded, the upper-bound of $B(q, \dot{q})$ can be obtained as

$$|\Delta B_1| \leq \left(\frac{1}{3}m_5a_5^2 - J_5\right)|\dot{q}_1 \cdot \dot{q}_2| \triangleq \delta_{B_1},$$

$$|\Delta B_2| \leq \left(\frac{1}{6}m_5a_5^2 - \frac{1}{2}J_5\right)|\dot{q}_1^2| \triangleq \delta_{B_2}.$$

Meanwhile, the upper-bound of $G(q)$ can be expressed as

$$|\Delta G_1| = 0,$$

$$|\Delta G_2| \leq \frac{1}{2}a_5gm_5 \triangleq \delta_{G_2}.$$

Finally, the upper-bound of $\dot{M}(q)$ can be derived by

$$\left|\Delta\dot{M}_{11}\right| \leq \left(\frac{1}{3}m_5a_5^2 - J_5\right) \cdot |\dot{q}_2| \triangleq \delta_{\dot{M}_{11}},$$

$$\left|\Delta\dot{M}_{12}\right| = \left|\dot{M}_{21}\right| = \left|\dot{M}_{22}\right| = 0.$$

5 Simulation and experimental results

The performance of the sliding-mode controller was verified numerically and experimentally using the experimental setup shown in Fig. 3. The antenna system parameters of interest include the followings.

$m_4 = 6$ (kg), $m_5 = 1.5$ (kg),
$a_4 = 0.55$ (m), $a_5 = 0.15$ (m)
$J_4 = 1.5 \times 10^{-2}$ (kg m^2), $J_5 = 3.75 \times 10^{-3}$ (kg m^2)
$g = 9.81$(m/sec^2).

Similarly, the parameters of the hydraulic platform are $d_1 = 0.72$ (m), $a_3 = 0.55$ (m) and $L = 1.10$ (m).

Parameters c_1' and c_2 in the control scheme were both assigned the value of 25 in order to ensure a satisfactory

convergence rate. Finally, the required azimuth and elevation angles of the antenna dish were specified as

$Az = 45°$ and $El = 45°$.

5.1 Numerical simulation results

According to (Liao 2001), a ship performs the following roll and pitch motions under normal sailing conditions:

$roll = \pm 7.5°$ at 0.08 Hz,

$pitch = \pm 4°$ at 0.16 Hz.

The corresponding motions are simulated and shown in Fig. 5. It assumed for simplicity the phases of the roll and pitch motions are identical.

Figure 6 illustrates the simulation results obtained for arm trajectories and input torque signals of arm-1 and arm-2 of the robotic structure. The commands of the arm trajectories are calculated for the aforementioned given roll and pitch motions of the ship and employment of the Denavit–Hartenberg (D–H) transformation described in Sect. 2.A. Also shown in figures are the arm torqueses and resulted responses of arm trajectories. It can be seen that the angles of both arms converge to the command values within 1.5 s. However, it can also be seen that the use of a sign function in the control rule causes a chattering phenomenon, which is often caused by inevitable noises involved in electronic operations. To remedy the problem, the sign function was replaced by the following saturation function

$$sat(s/\varepsilon) = \begin{Bmatrix} 1 & s > \varepsilon, \\ s/\varepsilon & -\varepsilon < s < \varepsilon, \\ -1 & s < -\varepsilon, \end{Bmatrix} \quad (34)$$

where ε is the boundary layer thickness. For the particular case of $\varepsilon_1 = \varepsilon_2 = 0.05$, Fig. 7 reveals that the trajectories of the two arms are considerably smoother when the saturation function is applied. Finally, Fig. 8 confirms that the application of the sliding-mode controller enables the ship-mounted satellite antenna not only to achieve the desired global orientation of $Az = 45°$ and $El = 45°$ (relative to ground) within 1.5 s, but also to maintain this orientation as the ship continues to pitch and roll, even the sensor signals may have noise.

5.2 Experimental results

Figure 2 presents the photograph of the major components used to construct the experimental satellite antenna/hydraulic platform system. Note that the detailed

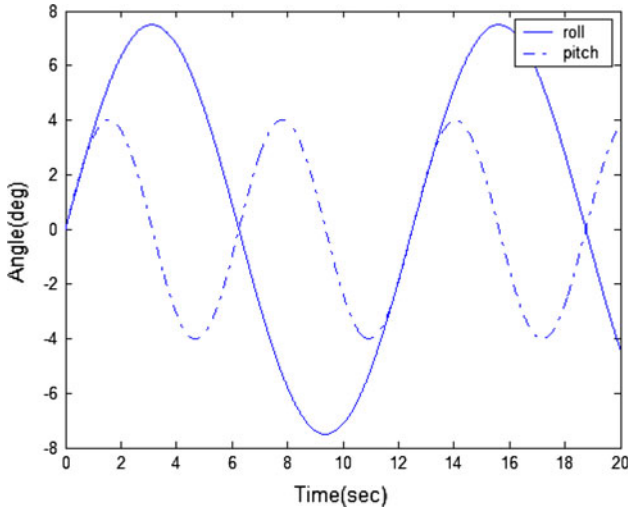

Fig. 5 Simulated roll and pitch motions of the ship

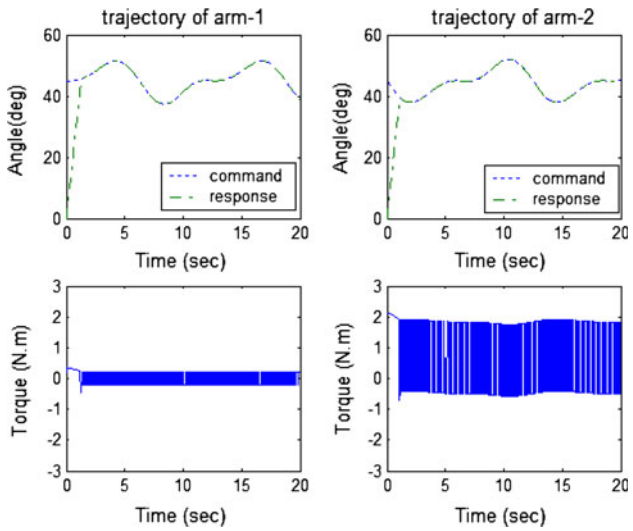

Fig. 6 Simulated response of the satellite antenna with sign function in control rule

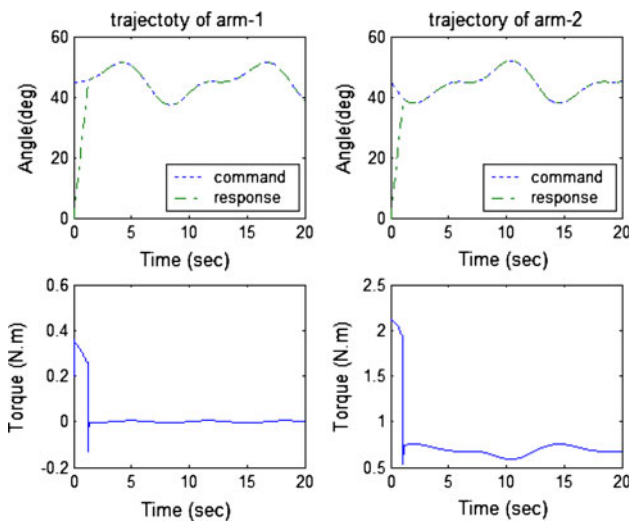

Fig. 7 Simulated response of the satellite antenna with the saturation functions in control rule

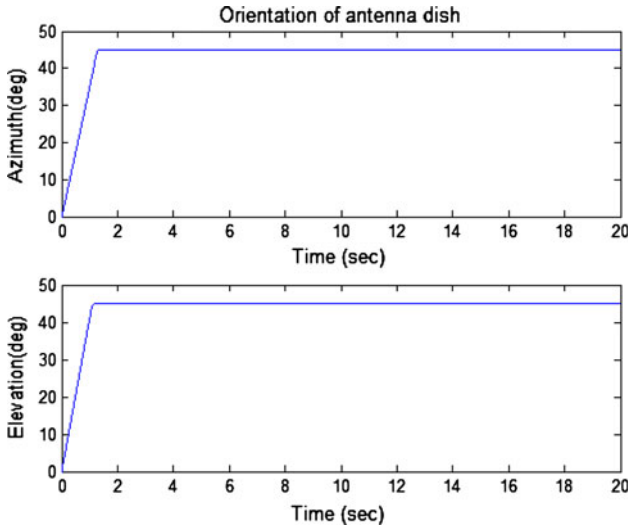

Fig. 8 Simulated orientation of the antenna dish relative to Earth's coordinate system

specifications of each component are summarized in Table 2. It is seen from this photo that the antenna dish is attached to a two-DOF robot mounted on a triangular platform supported by a rod with a universal joint at one corner and two hydraulic cylinders at the other two corners. The platform itself plays the role of the ship body. Roll and pitch motions of the ship are simulated by supplying appropriate driving signals to the AC motors used to actuate two cylinders, for the purpose of realizing corresponding roll and pitch angles of the platform supporting the antenna structure. The displacements of the two hydraulic cylinders are measured using linear potentiometers.

In the experiments, the control scheme was implemented using a DSPACE module. The control variables were the angles of arm-1 and arm-2 (measured using rotary potentiometers) and the displacements of the two hydraulic cylinders (measured using linear potentiometers). The measurement signals corresponding to these variables were supplied to the DSPACE module which then computed the torque signals required to regulate the two robotic arms such that the antenna dish remained aligned in the specified direction (i.e. $Az = 45°$ and $El = 45°$).

Figure 9 shows the experimental and commanded displacements of the two hydraulic cylinders required to achieve the pitch and roll motions defined in Sect. 5.1. Note that these commanded cylinder displacements are computed based on the two transformations developed in Sect. 2 A and B, which are used to calculate the desired cylinder displacements from given roll and pitch motions of the ship. Figure 1 also illustrates the computation process. On the other hand, experimental cylinder displacements are also shown, the closeness of which with the

Table 2 Description and specification of experimental apparatus

Components	Specifications
Hydraulic power unit	AC 220 V motor, 1/2 HP
	Max output pressure: 70 (*bar*)
Hydraulic cylinder	Piston area: 12.56 cm^2
	Stroke: 200 mm
Proportional-valve	Max work pressure: 350 (*bar*)
Panasonic AC servo motor	Max output torque: 7.1 N m
Proportional-valve	Max work pressure: 350 (*bar*)
Rotary potentiometer	Effective measured rang: 300°
	Resolution: 0.05°
Linear potentiometer	Electrical stroke: 200 mm
	Resolution: 0.01 mm

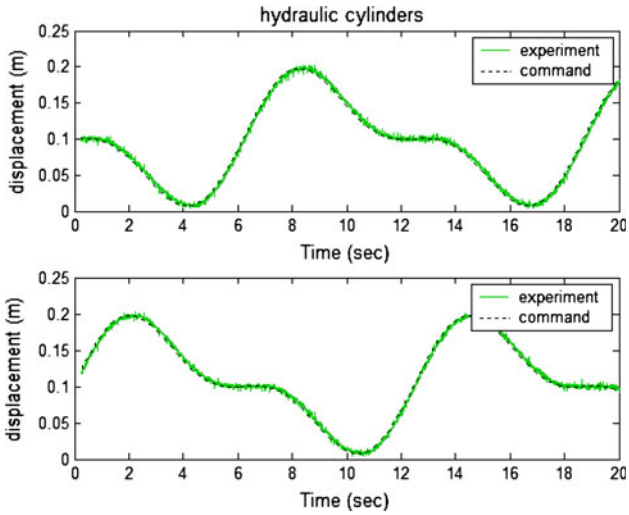

Fig. 9 Experimental displacement of hydraulic cylinders

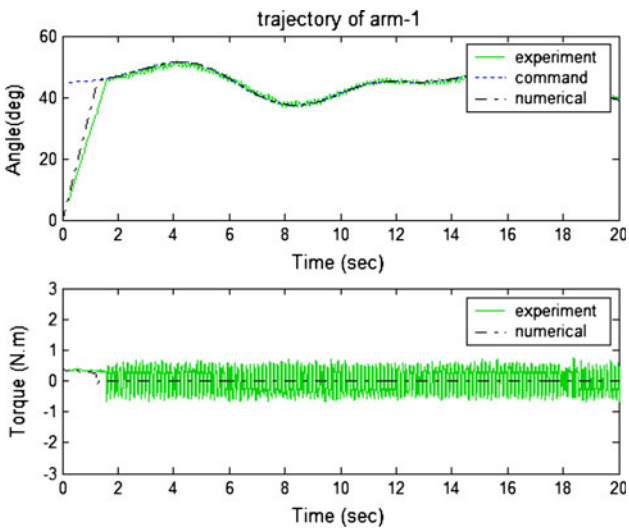

Fig. 10 Experimental and numerical results for displacement and torque of the arm-1

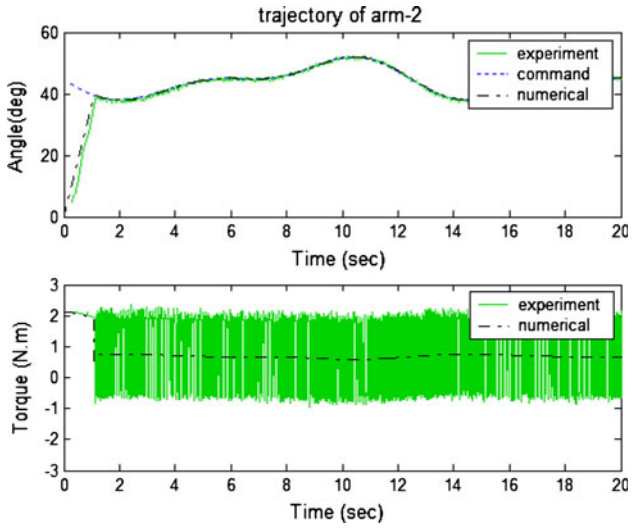

Fig. 11 Experimental and numerical results for displacement and torque of the arm-2

command counterparts are present, showing satisfactory motions precision of the built platform mechanism.

Figures 10 and 11 present the experimental results for the trajectories and torque signals of arms 1 and 2, respectively. Figure 12a shows the corresponding variations of the azimuth and elevation angles of the antenna dish, and Fig. 12b illustrate schematically the postures of the ship-carried satellite antenna. At time 1 ($t = 0$), no controlled torque is applied, while at time 2–4 the designed sliding-mode controller is applied to maintain the antenna in a specified orientation, while the ship pitches and rolls under the combined effects of wind and sea waves. Note in these figures that corresponding numerical results are presented for comparison purposes. It is seen from Figs. 10 and 11 that a clearly good agreement is present among command, numerical and experimental data of arm angles, showing the effectiveness of the proposed sliding-mode controller designed in this study. However, the chattering is still present in experimental torque data, despite the use of a saturation function in the control rule. This is due to much larger control signal noises embedded in practical actuating hydraulic cylinders and other platform components. Finally, Fig. 12a shows global orientation angles of the antenna, where the strong agreement between the experimental data and numerical counterparts are clearly seen. On the other hand, subfigure (b) illustrates the gestures of the ship-carried satellite antenna at time 1 ($t = 0$) when no controlled torque is applied, and at time 2 ($t = 1$), time 3 ($t = 1.5$) and time 4 ($t = 2$) when the designed sliding-mode controller is applied

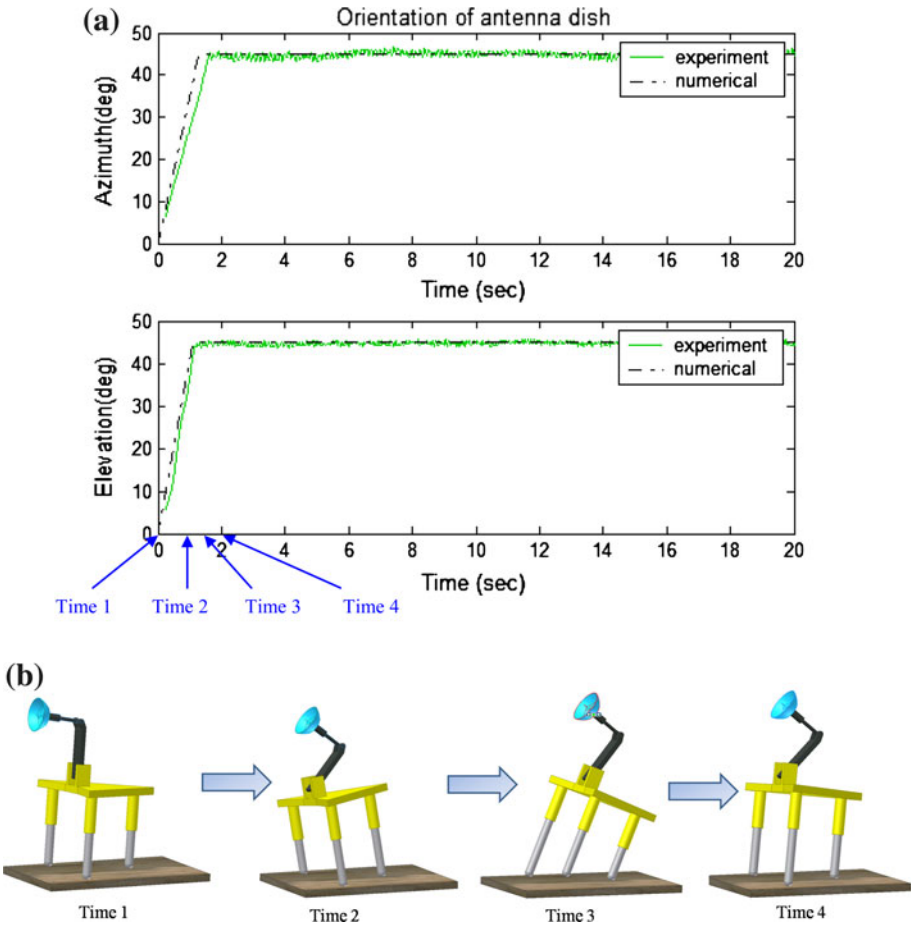

Fig. 12 **a** Experimental azimuth and elevation angles of the antenna dish; **b** illustration the of the ship-carried satellite antenna at time 1 ($t = 0$) when no controlled torque is applied; at time 2 ($t = 1$), time 3 ($t = 1.5$) and time 4 ($t = 2$) when the designed sliding-mode controller is applied to maintain the antenna in a specified orientation relative to earth

to maintain the antenna in a specified orientation relative to earth. It is also noted from subfigures (a) that the times required for the experimental system to converge to the required antenna dish orientation is slightly longer than that predicted numerically, i.e. 2 s rather than 1.5 s.

6 Conclusion and future studies

This study has developed a sliding-mode controller to stabilize a ship-mounted satellite antenna as the ship performs non-linear roll and pitch motions. The performance of the controller has been demonstrated numerically and experimentally. Both sets of results have confirmed the feasibility of the proposed control scheme. The antenna converges to the required azimuth and elevation angles within 2 s and then maintains the specified orientation as the ship continues to pitch and roll. The numerical results have shown that the chattering effect observed in the response of the controlled antenna system can be eliminated via the use of a saturation function in the control rule. However, the chattering phenomenon still remains in the experimental results even when the boundary layer thickness of the saturation function is broadened. Chattering is undesirable in the present system since it degrades the quality of the signals received from the positioning satellite. It is probably due to the fact that this chattering effect stems partly from the noises embedded in practical actuating hydraulic cylinders and other platform components. Consequently, a future study will attempt to suppress the steady state positioning errors induced by chattering by sliding-mode controller.

Acknowledgments The authors are greatly indebted to the National Science council of R.O.C. for the support of the research through contracts in Nos. NSC96-2220-E-009-029 and 96-2622-E-009-010-CC3. This work was also supported in part by the UST-UCSD International Center of Excellence in Advanced Bio-Engineering sponsored by the Taiwan National Science Council I-RiCE Program under Grant NSC-100- 2911-I-009-101.

References

Bailey E, Arapostathis A (1987) Simple sliding mode control scheme applied to robot manipulators. Int J Control 45(4):1197–1209

Chen SL (1993) Molding dynamics and control of larger amplitude motion of vessel in beam seas, Ph.D Thesis, Department of Mechanical Engineering, Michigan State Univerity

Chen YF, Mita T, Wakui S (1990) A new and simple algorithm for sliding mode trajectory control of the robot arm. IEEE Trans Autom Control 35(7):828–829

Chris Tseng H, Teo Dennis W (1998) Ship-mounted satellite tracking antenna with fuzzy logic control. IEEE Trans Aerosp Electron Syst 34(2):639–645

Jung-Huang Liao (2001) The design of radar stabilized pedestal, Master Thesis, National Tsing Hua University

Schilling Robert J (1990) Fundamentals of robotics analysis and control. Prentice-Hall, Canada

Slotine JJ (1984) Sliding controller design for non-linear systems. Int J Control 40(2):421–434

Spong Mark W, Vidyasagar M (1988) Robot dynamic and control. Wiley, New York

Spong MW, Vidyasagar M (1989) Robot dynamics and control. Wiley, New York

Yeung KS, Chen YP (1988) A new controller design for manipulators using the theory of variable structure systems. IEEE Trans Autom Control 35(7):200–206

KD Young (1978) Controller design for a manipulator using theory of variable structure systems. IEEE Trans Sys, Man, Cybern SMC-8:101–109